Sugar: Advancements in a 3D Multi-domain Simulation Package for MEMS

J.V. Clark, D. Bindel, N. Zhou, S. Bhave, Z. Bai, J. Demmel, K.S.J. Pister

Berkeley Sensor & Actuator Center
University of California at Berkeley, Berkeley, CA, USA
497 Cory Hall, jvclark@eecs.berkeley.edu

ABSTRACT

Advancements in Sugar include 1) parameterizable netlists, 2) nonlinear frequency response analysis, 3) subnets, 4) improved MNA, 5) reduced order modeling, and 6) a more accurate nonlinear beam model. Examples of these features include the simulation of a two-axis mirror with over 10,000 degrees of freedom, the reduced order modeling applied of an electrostatic gap actuator, the parameterized deflection space of a thermal actuator and serpentine flexure, and the nonlinear response of a fixed-fixed beam.

Keywords: Modified nodal analysis, modeling, Sugar, simulation.

1 INTRODUCTION

As we witness the unfolding of the micromachine revolution, microelectromechanical systems are moving from simple single function devices to elaborate systems with complex characteristics. However, MEMS designers are continually bumping up against the limits of finite element analysis due to the ceiling imposed by computer processing power. Despite the number of CAD products available, some designers still find it easier to approximate design solutions by hand rather than delve into the rigorous details of the software.

Sugar [1] was created to investigate remedies to the above problems. To alleviate computer processing and memory requirements we have shown that the number of equations that described many designs can be greatly reduced using modified nodal analysis while still maintaining accuracy within fabrication limits [2]. The test cases included the warping of an ADXL05 accelerometer due to residual stress and strain gradients, process variation analysis where the possible displacement distributions and worst case scenarios were predicted, the transient response of a gyroscope in an accelerated frame of reference, electrical currents induced by multimode resonators, and thermal actuation to name a few.

We have also demonstrated that MNA systems can be further reduced by a reduced order modeling method based on Krylov subspaces and numerical accuracy improved by scaling schemes [3]. Similar promising research in this area includes network analysis [4-5] and macromodeling [5-6].

User-friendliness is a major obstacle for both the CAD developer and the CAD user due to the inherent multiphysics nature of MEMS, e.g. electronics + mechanics + fluidics + thermal + etc. For the ease of use we chose to exploit the popular Matlab™ software. This familiar open-code environment invites modifications, features, and additional remedies from users.

Addressing the needs listed above, this paper shows progress toward effectively raising the "computational ceiling." What is gained is the ability to simulate much larger systems faster. To show that sophisticated system design can made simple we demonstrate how complex designs, which may consist of thousands of components, can be reduce down to just a few lines of netlist text with the aid of parameterized subnets. Lastly, mechanical nonlinearity has gained substantial interest with the MEMS designer and has been historically problematic in lumped structural analysis. We present recent results for a new nonlinear beam model.

2 MULTI-DOMAIN REPRESENTATION

It is well known that the dynamics of many physical processes can be described by a system of second order ODEs of the form (1). For a purely mechanical system, the matrices M, D, and K are identified with mass, damping, and stiffness. The vectors q and F are the state and excitation.

$$M\ddot{q} + D\dot{q} + Kq = F(t, q, \dot{q}) \qquad (1)$$

Modified nodal analysis, as used in Spice™, has proven to be effective for matrix circuit analysis. Sugar extends the use of MNA to the special case of multi-energy domains inherent to MEMS. To formulate an MNA equation, elements of the domains are resolved into three groups. The first group contains elements that have a natural nodal analysis representation and whose sates do not need to appear in the MNA solution vector. The second group consists of elements

that do not have a nodal analysis representation or whose states are to appear in the MNA solution vector. Independent sources live in the third group. The MNA equation is assembled as follows. Group 1 states enter the MNA matrix in terms of their admittance. Group 2 states are entered as components in the solution vector, which add a constraint equation (CE) to the system. For example, the mechanical MNA representation of (1) is

$$\begin{bmatrix} M & D \\ 0 & I \end{bmatrix} \begin{bmatrix} \ddot{q} \\ \dot{q} \end{bmatrix} = \begin{bmatrix} 0 & -K \\ I & 0 \end{bmatrix} \begin{bmatrix} \dot{q} \\ q \end{bmatrix} + \begin{bmatrix} F \\ 0 \end{bmatrix} \qquad (2)$$

For electronics we have

$$\begin{bmatrix} G & CE_2 & C_2 \\ CE_1 & 0 & 0 \\ C_1 & 0 & 0 \end{bmatrix} \begin{bmatrix} V \\ \dot{Q} \\ \dot{V} \end{bmatrix} = A_{mx} \begin{bmatrix} W \\ Q \\ V \end{bmatrix} + B_{ms} \begin{bmatrix} 0 \\ V \\ 0 \end{bmatrix} \qquad (3)$$

In MEMS, equation (2) and (3) are coupled. E.g. voltage differences in (3) generate nodal forces in (2); at the same time, displacements in (2) change capacitances in (3).

Combining (2) and (3) into a single equation (4), the complete first order system is given by (5).

$$G_{mna} \dot{X} = A_{mx} X + B_{ms} f(X, \dot{X}, t) \qquad (4)$$

$$\dot{X} = AX + Bf(X, \dot{X}, t) \qquad (5)$$

where G is the conductance matrix, G_{mna} is the multidomain MNA matrix, $\dot{X}$ is the solution vector, X is the state vector, A & B are coupling matrices, C is capacitance, V is voltage, W is time-integral of V, and Q is charge [1].

The following example demonstrates the coupling of electronic, mechanic, and electrostatic domains. The results of static and transient pull-in are provided in Figures 1-4.
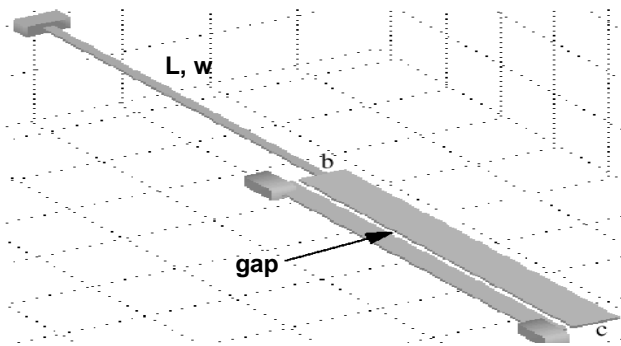
Figure 1: As a voltage difference is applied across the gap (capacitor), nodal forces and moments are generated. The flexible beams are also modeled as electronic resistors. Air between the structure and substrate provide viscous damping.
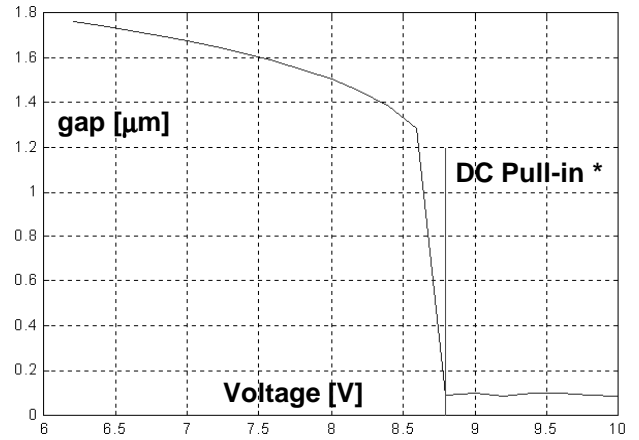
Figure 2: gap displacement of node c, versus voltage across gap. *Due to a finite iterative step in the DC solver, the pull-in point is not shown as vertical.
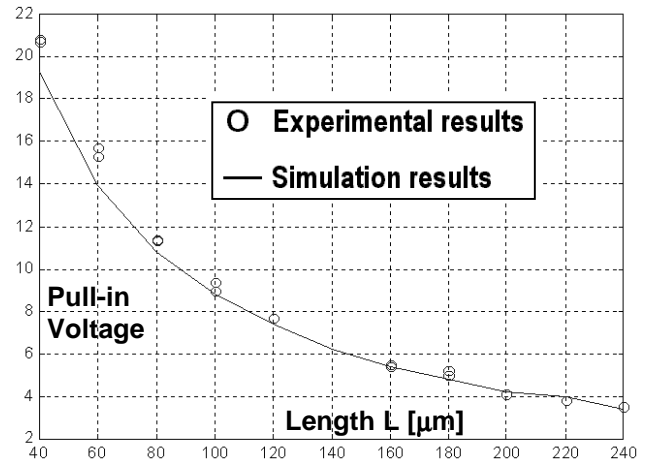
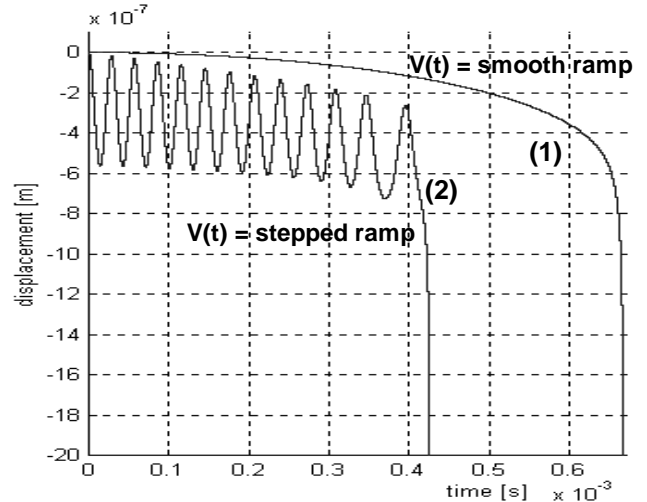**Figure 3:** Pull-in voltage versus beam length L. w = 1.74um, h = 2.003um, Young's modulus = 165GPa.

Figure 4: Two transient responses of pull-in. (1) A smooth voltage ramp pulls in at 2/3-gap distance. (2) An abrupt stepped ramp induces oscillation. Note the nonlinear period due to increasing electrostatic forces.

Krylov subspace methods are emerging numerical techniques for reduced-order modeling of large-scale dynamical systems. They have lead to a major breakthrough in the field; see, for example, the survey paper [8] and the references therein. The need and challenges of reduced order modeling techniques for simulating MEMS devices are discussed in [9]. Details concerning the formulation of reduced-order modeling in Sugar can be found in [3]. Figures 5 shows a superimposed reduced-order simulation over our general transient solver. The voltage ramps from 5V at t=10µs to 12V at t=500µs, and then drops to 0V. Relative errors of the reduced models of order n=2 and n=6 are shown in Figure 6. The order of the original system is N = 30. Using a SUN 440MHz Ultra 10, the simulation times where 2s, 428s and 28ks respectively using the Matlab ode15s, stiff ODE solver.
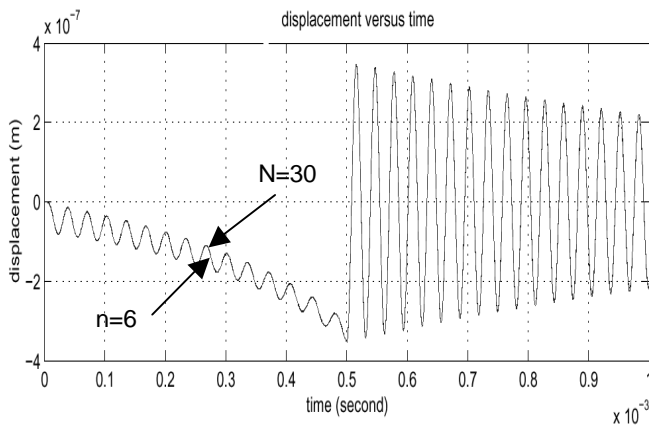

Figure 5: *Reduced order modeling simulation (6th order) superimposed onto our general transient solver (30th order) qualitatively demonstrates accuracy. The lower dimensionality of the reduced order system decreased the simulation time by a factor 1/60.*
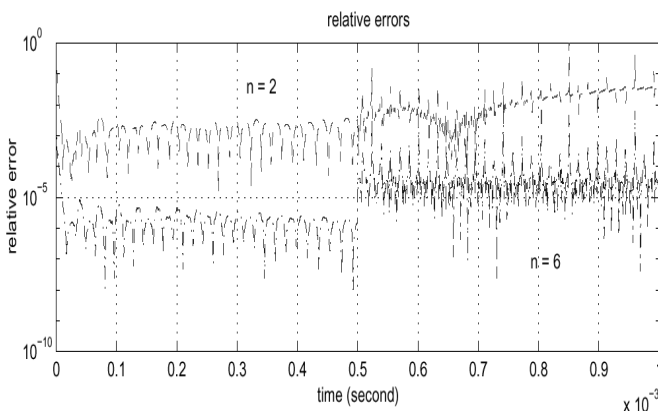

Figure 6: *Relative errors of reduced-order modeling for a 2nd order (top) and 6th order model (bottom).*

3   SUBNETS & PARAMETERIZATION

Figure 7A shows a laterally actuated high aspect ratio torsionally suspended micromirror [10]. It consists of a circular mirror (center) and several hundred comb-drive fingers that supply the lateral force necessary to rotate the mirror out of plane. Figure 7B shows a view from the side. A close-up of a

hinge assembly is given in Figure 7C. The comb-drive array generates a load on the hinge. This load is applied below the axes of rotation, thus producing a moment that results in out-of-plane rotation of the circular mirror. Compliance in the structure also produces an undesired lateral displacement.

As modeled in Sugar this device has 10,026 degrees of freedom and 4,118 beam elements. The complex interplay of the hinge assembly alone makes hand analysis difficult. Likewise, large systems can hinder CAD users because the increased occurrence of design errors. A solution to both problems is the use of subnets, which can reduce large netlists down to just a few lines of text. In Figure 7A, the comb-drive array, center ring, and hinges are subnets. Each subnet occupies a single line of netlist text. For versatility, subnets may be parameterized, contain simple mathematical operations, and nested loops.
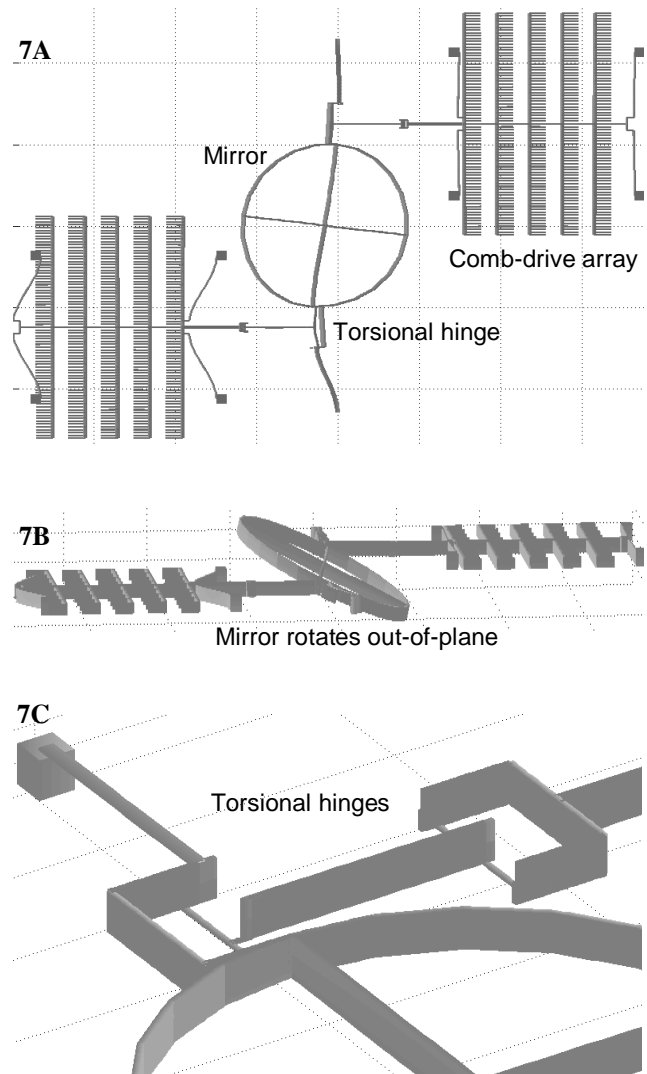

Figure 7: *Simulation of a torsional micromirror. 7A and 7B show a slightly exaggerated deflection of the out-of-plane tilt of the center mirror. 7C shows the complicated hinge assembly. DC simulation of this 10,000 degree of freedom device takes just under 2 minutes using a PIII-800MHz. After subnets are defined, the netlists is just 17 lines of code.*

Variations in geometry and material properties may also be imposed at the Matlab command line instead of inside the netlist. In this manner, changing the number of comb-drive fingers, the width of the torsional hinges, or the Young's modulus in the above design becomes trivial. This allows the parameters to be swept to characterize their sensitivity. Figure 8 shows the primary mode shape of a serpentine flexure. The frequency of this mode is governed by the effective stiffness along the y-axis and the effective mass, which includes the heavy center square and small contributions from the meandering springs. If there are size constraints imposed on a device, it becomes necessary to examine different geometry's while still maintaining certain performance properties. Figure 9 shows level curves of effective stiffness as a function of width and length of the serpentine flexure. The axes represent changes in length and width from fabricated dimensions given in [11].
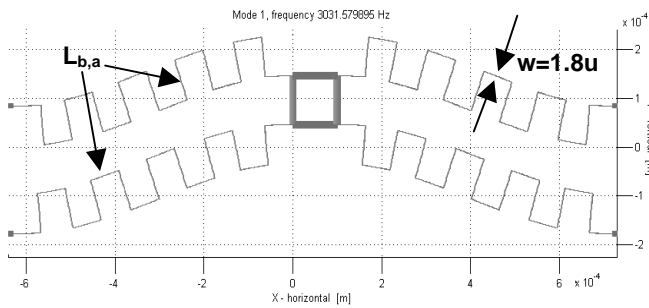

Figure 8: *Modal analysis of a serpentine flexure. Primary mode results: Experimental 2697Hz [11], Finite Element Analysis 3032Hz, Sugar 3032Hz. Sugar matches FEA; however, both simulations overestimate primary resonance due to the absence of damping during simulation.*
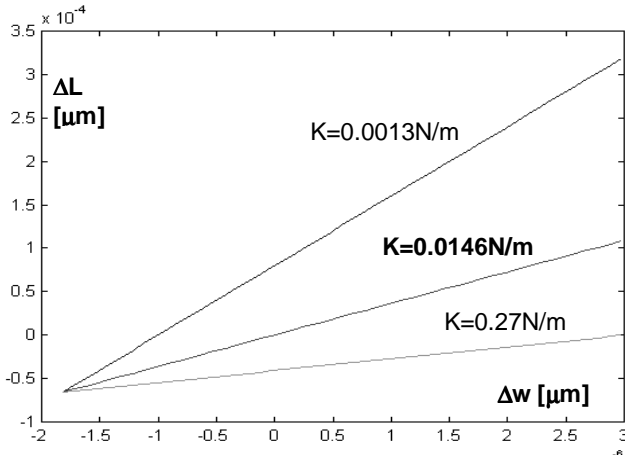

Figure 9: *ΔL versus Δw, producing level curves of stiffness for the serpentine flexure. For fabricated dimensions, the simulated stiffness of 0.0146N/m exactly matches FEA and is within 1.2% of the measured stiffness [11].*

It is often customary to optimize performance by adjusting material properties or geometry. Figure 10 shows the simulated deflection of a thermal actuator. The geometry and average beam temperature were measured by [11]. Before actuation the device is

horizontal. As current passes through the beams, the slender beam heats up more than the thick beam due to a smaller cross-section, which results in higher resistance. This generates a larger thermal expansion of the slender beam, causing the tip to deflect downward. The small gap spacing encourages this deflection; yet the restoring spring force of the beams oppose it. Figure 11 explores the space of the deflected tip by pitting the gap g against the beam width w. Here it is assumed that the temperatures remain.
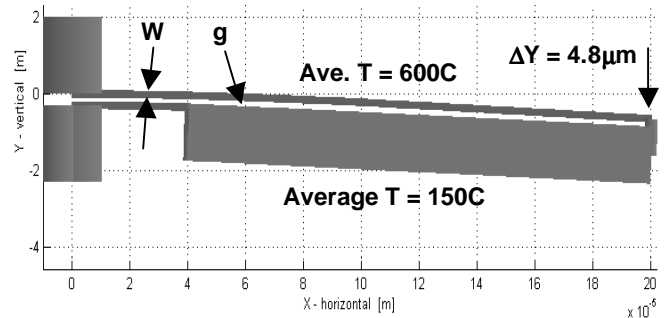

Figure 10: *Thermal actuator. In the real device there's a heat distribution along the hot and cold arms, however, averaging the temperature along the beam produces the same overall linear thermal expansion. SUGAR is within 0.5% of the measured deflection [12].*
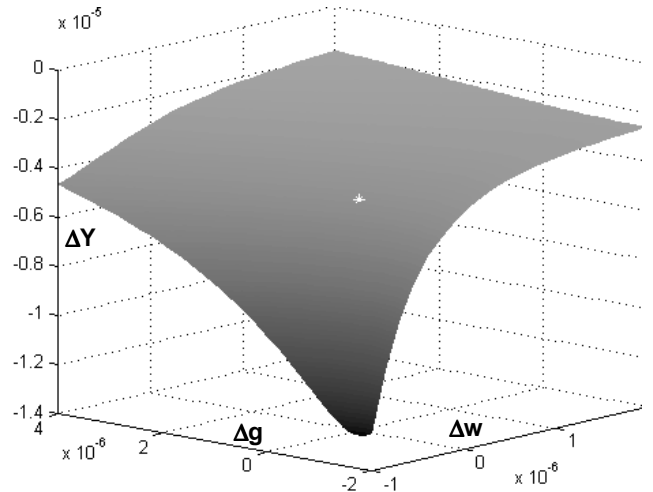

Figure 11: *Tip deflection ΔY as a function of change in gap space Δg and change in width Δw. This design space reveals where geometry may be optimized for maximum deflection, given the limits of the process design rules.*

4   NONLINEAR RESPONSE

Linear beams have been well characterized [2,11]. The use of linear beam models in designs has been widely preferred over nonlinear beams since they are easier to analyze. But linear models are typically valid for only small deflections. For MEMS that are subject to large deflections or extremely

sensitive devices such as accelerometers and gyroscopes [13], approximations using small deflection theory may no longer hold.

The first results[1] of an improved nonlinear beam model are given here. Figure 12 shows the deflection of a beam constrained at the end nodes. All relevant terms are defined as well. As a force is applied to the center node, there is an increased stiffening of the beam primarily due to its change in length. In contrast, the stiffness of linear models remains constant during deflection, Figure 13.
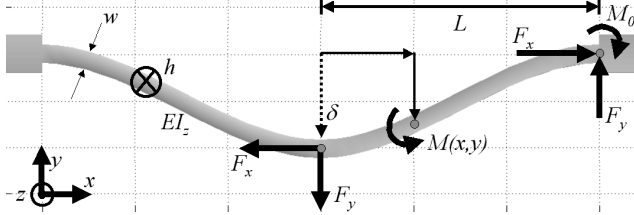
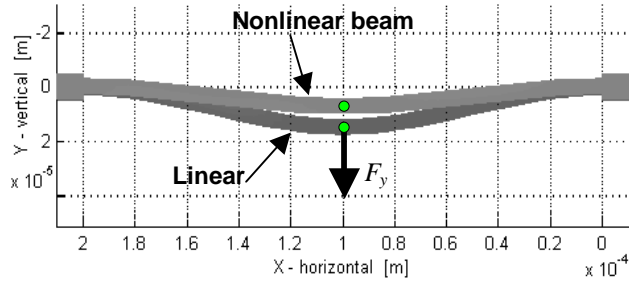**Figure 12:** *Nonlinear beam quantities defined. See equations (6) – (10).*

Figure 13: *Contrasting a linear deflection against a nonlinear deflection for the same applied force. The restoring force of nonlinear beams is approximately cubic in displacement; the stiffness of the linear beam stays constant during displacement.*

If curvature is small, the moment at any position along the nonlinear beam in Figure 12 is

$$M(x, y) \approx EI_z \frac{d^2 y}{dx^2} = F_x y + M_0 - F_y(L - x) \quad (6)$$

$$\text{where} \quad I_z = \frac{w^3 h}{12} \quad (7)$$

By applying suitable boundary conditions to (6), it can be shown [1] that the governing nodal equations are

$$\lambda = \frac{L}{2} \sqrt{\frac{F_x}{EI_z}} \quad (7)$$

$$"F_y" = \frac{F_y L^3}{EI_z} \sqrt{\frac{A}{I_z}} = \frac{\lambda^3 8\sqrt{2}}{\sqrt{\frac{3}{2} - \frac{1}{2}\tanh^2 \lambda - \frac{3}{2}\frac{\tanh \lambda}{\lambda}}} \quad (8)$$

---

[1] This model is currently in the developmental stage.

$$"\delta" = \delta \sqrt{\frac{A}{I_z}} = \frac{2\sqrt{2}(\lambda - \tanh \lambda)}{\sqrt{\frac{3}{2} - \frac{1}{2}\tanh^2 \lambda - \frac{3}{2}\frac{\tanh \lambda}{\lambda}}} \quad (9)$$

$$"M" = \frac{M_0 L^2}{EI_z} \sqrt{\frac{A}{I_z}} = \frac{\lambda^3 4\sqrt{2}\tanh \lambda}{\sqrt{\frac{3}{2} - \frac{1}{2}\tanh^2 \lambda - \frac{3}{2}\frac{\tanh \lambda}{\lambda}}} \quad (10)$$

Equations (7) – (10) are nondimensionalize for generality. They represent the nodal axial force (7), transverse force (8), deflection (9), and moment (10). A plot of (7) – (10) is provided in Figure 14. Choosing λ for (7) and plugging that value in to equations (8) – (10) generates them. Dividing (8) by (9) gives the nonlinear stiffness.
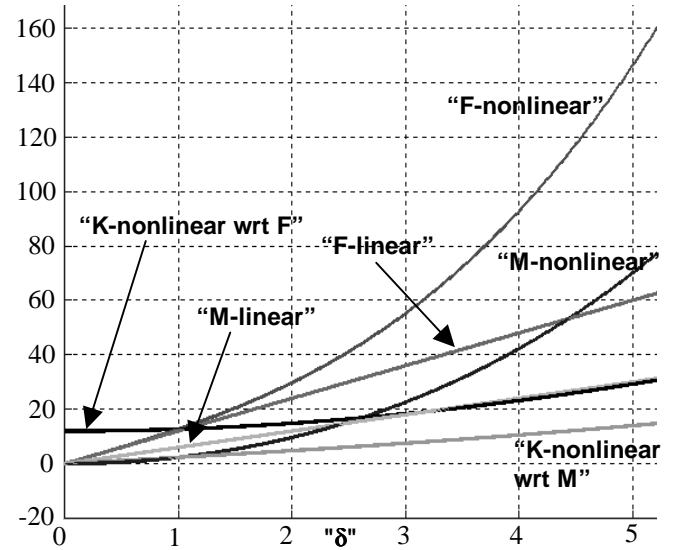
Figure 14: *Plots of nonlinear node quantities in nondimensional units for a fixed-fixed beam. The plot shows the nonlinear & linear force, moment, and stiffness as functions of deflection.*

For an improved nonlinear model, we fit a cubic equation to these results. Since such a fit is only valid within a finite range of deflection we use a piecewise continuous form (11), where K_{lin} is the constant linear stiffness used in our linear beam model, and $K_{nl,i}$ is the nonlinear stiffness for the ith range of deflection.

$$F_0 = K_{lin} q + K_{nl,i} q^3 \quad (11)$$

Using this method we are able agree with the entire range of theory to the desired accuracy, Figure 14.

To obtain a nonlinear frequency response we currently decouple the system equation [14] and use the method of multiple scales [15] on a particular degree of freedom. For a cubic equation driven near primary resonance by a sinusoidal excitation of the form F(t) = F_0 cos(ωt), the detuning is given by, [1]

$$\Omega = \frac{3}{8}\frac{K_{nl}'}{w_0}q_{max}^2 \pm \sqrt{\frac{F_0'^2}{4w_0^2 q_{max}^2} - \frac{D'}{2}} \qquad (12)$$

where the primes denote said quantities divided by an effective mass. The + and – in (12) correspond to the stable (upper branch) and semi-unstable (lower branch) curve in Figure 15. This multivaluedness is responsible for the *jump phenomena* often seen in nonlinear structures. The central backbone to the curve in Figure 15 is given by the first term in (12). The maximum amplitude at peak resonance can be shown [1] to be

$$A_{max} = \frac{F_0'}{w_0 D'} \qquad (13)$$

which is independent of K_{nl}. Sugar demonstrates that the effect of the K_{nl} nonlinearity is to bend the amplitude curve and distort the phase curve causing the multivalued regions, Figures 15 and 16.
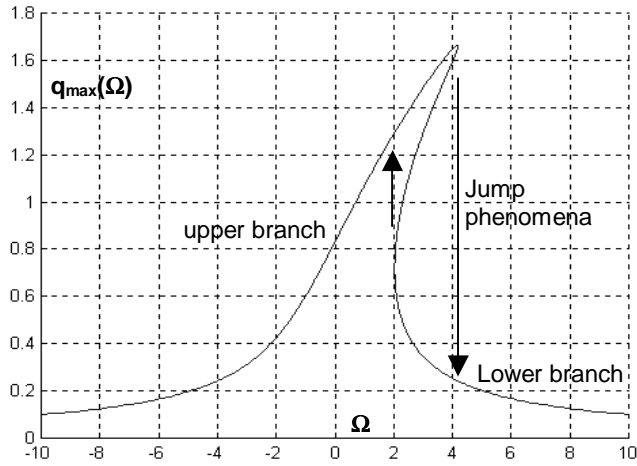

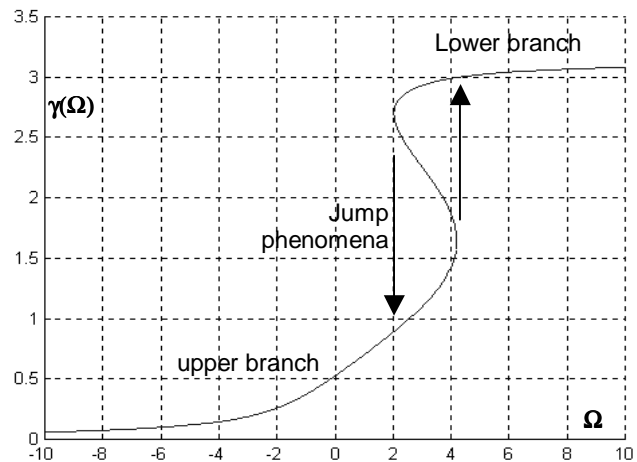**Figure 15:** *Nonlinear frequency response curve shows maximum displacement as a function of frequency detuning.*

Figure 16: *Phase plot.* $\gamma = \cos^{-1}\left[\frac{2\omega_0}{F_0}\left(\frac{3}{8}\frac{K_{nl}'}{\omega_0}q_{max}^3 - q_{max}\,\Omega\right)\right]$

REFERENCES

[1] *Sugar*, CAD for MEMS, publications, presentations, and software, http://www-bsac.eecs.Berkeley.edu/~cfm.

[2] Clark JV, Zhou N, Bindel D, Schenato L, Wu W, Demmel J, Pister KSJ, *3D MEMS Simulation Modeling Using Modified Nodal Analysis*, Proc of the Microscale Systems: Mechanics and Measurements Symposium, pp 68-75, June 8, 2000, Orland Florida.

[3] Bai Z, Bindel D, Clark JV, Demmel J Pister KSJ, Zhou N, *New Numerical Techniques and Tools in Sugar for 3D MEMS Simulation*, Tech Proc 4rd Intl Conf On Modeling and Simulation of Microsystems, March 2001, Hilton Head Island SC, USA.

[4] Fedder GK, *Top-Down Design of MEMS, Tech Proc 3rd Intl Conf On Modeling and Simulation of Microsystems,* pp 7-10, March 2000, San Diego CA, USA.

[5] Gollee R, Rabinovich VL, *A FEM Based Network Approach for the Simulation of Miniaturized Electromagnetic Devices*, Tech Proc 3rd Intl Conf On Modeling and Simulation of Microsystems, pp 221-224, March 2000, San Diego CA, USA.

[6] Senturia SD, Varghese M, *Reduced-order Models of Stress-Stiffend MEMS Structures*, Tech Proc 3rd Inter Conf On Modeling and Simulation of Microsystems, pp 493-496, March 2000, San Diego CA, USA.

[7] Lee HJ, Crary SB, et al, *Generation of a Metamodel for a Micromachined Accelerometer Using T-Spice™ and the Iz-Optimality Option of I-OPT™*, Tech Proc 3rd Intl Conf On Modeling and Simulation of Microsystems, pp 201-204, March 2000, San Diego CA, USA.

[8] Freund RW, *Reduced-order modeling techniques based on Krylov subspaces and their use in circuit simulation, Applied and Computational Control, Signals, and Circuits,* Vol. Q, pp435-498. Birkhauser, Boston, 1999.

[9] Senturia SD, *Simulating the Behavior of MEMS Devices: Computational Methods and Needs*. IEEE Computatinal Science and Engineering, 4:30-43, 1997

[10] Melanovic V, Last M, Pister KSJ, *Torsional micromirros with later actuators*, Transducers 01, Muenchen, Germany, June 2001

[11] Fedder GK, *Simulation of microelectromechanical systems*, PhD dissertation, UC Berkeley, 1994.

[12] Allen P, Howard J, Kolesar E, Wilken J, *Design, Finite Element Analysis, and Experimental Performance Evaluation of a Thermally-Actuated Beam Used to Achieve Large In-Plane Mechanical Deflection*, Tech Digest, Solid-state Sensor and actuator workshop, Hilton Head Island SC, pp191-196, June8-11, 1998.

[13] Lorenz Gunar, *Coventor*, personal communication.

[14] Buchholdt HA, *Structural Dynamics for Engineers,* Thomas Telford Pub, NY, 1997.

[15] Nayfeh AH, *Nonlinear Oscillations*, John Wiley & Sons Inc NY, 1979.